Graphene self-switching diodes as zero-bias microwave detectors

A. Westlund,[1,a)] M. Winters,[1] I. G. Ivanov,[2] J. Hassan,[2] P.-Å. Nilsson,[1] E. Janzén,[2] N. Rorsman,[1] and J. Grahn[1]
[1]*Department of Microtechnology and Nanoscience—MC2, Chalmers University of Technology, Gothenburg, SE-412 96, Sweden*
[2]*Department of Physics, Chemistry and Biology, Linköping University, SE-581 83 Linköping, Sweden*

(Received 23 January 2015; accepted 25 February 2015; published online 6 March 2015; corrected 17 March 2015)

Self-switching diodes (SSDs) were fabricated on as-grown and hydrogen-intercalated epitaxial graphene on SiC. The SSDs were characterized as zero-bias detectors with on-wafer measurements from 1 to 67 GHz. The lowest noise-equivalent power (NEP) was observed in SSDs on the hydrogen-intercalated sample, where a flat NEP of 2.2 nW/Hz$^{1/2}$ and responsivity of 3.9 V/W were measured across the band. The measured NEP demonstrates the potential of graphene SSDs as zero-bias microwave detectors. © *2015 AIP Publishing LLC*. [http://dx.doi.org/10.1063/1.4914356]

Graphene exhibits electronic properties which are relevant for high-frequency applications[1] such as zero-bias detection in passive imaging arrays.[2] Detectors drawing zero bias current offer reduced 1/f-noise compared to biased detectors. Zero-bias detectors are today normally based on heterojunctions or Schottky diodes, reaching noise-equivalent power (NEP) below 20 pW/Hz$^{1/2}$ beyond 100 GHz.[3,4] Zero-bias detection has been demonstrated in graphene field-effect transistors (FETs) with an NEP of 515 pW/Hz$^{1/2}$ at 600 GHz.[5]

Self-switching diodes (SSDs) offer a fundamentally different approach to zero-bias detection in which rectification and detection is achieved by a lateral field-effect.[6] Simulations have shown the feasibility of achieving rectification in graphene using SSD structures.[7,8] SSD detectors have previously been realized in other materials[9–12] with the most promising results for GaAs SSDs in which an NEP of 330 pW/Hz$^{1/2}$ at 1.5 THz was observed.[13] In this work, detection with rectifying graphene SSDs at frequencies up to 67 GHz is demonstrated. The SSDs are realized in both as-grown (n-type) and hydrogen-intercalated (p-type) epitaxial graphene on SiC.

Figure 1 shows a scanning electron micrograph of a single SSD channel fabricated in epitaxial graphene. The narrow graphene channel behaves as a lateral nanowire transistor.[6] The surrounding flanges act as lateral gates which are directly connected to the drain such that the drain voltage is simultaneously applied to the gates. This has the effect of modulating the carrier density in the nanowire channel generating a nonlinear current-voltage characteristic.[14] The inset shows an SSD design implemented for RF detection with nine nanowire channels acting in parallel to reduce resistance and NEP.[15] The SSDs were fabricated at the end of a 70 μm coplanar transmission line, in order to provide a partial RF match.

Graphene was grown on the Si-face of two 20×20 mm^2 nominally on-axis semi-insulating (SI) 4H-SiC substrates in a horizontal hot wall chemical vapor deposition (CVD) reactor.[16] Graphene growth was carried out at 1300 °C to 1400 °C in vacuum after an initial *in-situ* surface preparation of the substrates in a hydrogen/silane background. One of the samples was then intercalated in hydrogen at a temperature (pressure) of 800 °C (500 mbar) in order to obtain quasi-free standing graphene. SSDs and supplementary test structures were fabricated on the graphene layers with and without H-intercalation. As-grown samples then consisted of a monolayer plus carbon buffer layer (CBL), and samples which were intercalated with hydrogen consisted of quasi-free standing graphene bilayers.[17–19]

Processing began by patterning the SSD flange structures via electron beam lithography (EBL). The flanges were then etched in O_2 plasma. Ti/Au ohmic contacts were deposited and mesas etched via O_2 plasma followed by the definition of Ti/Au contact pads.[20] In order to prevent long term sample degradation, an encapsulation using benzocyclobutene (BCB) diluted in (1,3,5) trimethylbenzene (1:4) was done.[20] Hall measurements yielded an average mobility (carrier density) of 1392 cm^2/Vs ($-6.91 \cdot 10^{11}$ cm^{-2}) for the as-grown material and 1130 cm^2/Vs ($+1.95 \cdot 10^{13}$ cm^{-2}) for H-intercalated material. This corresponds to mean Fermi energies of $\epsilon_f = 88$ meV (-366 meV) for the as-grown (H-intercalated) samples, respectively.[21] The measured mobilites and sign of the majority carriers for as grown and H-intercalated material are consistent with previous results.[20]

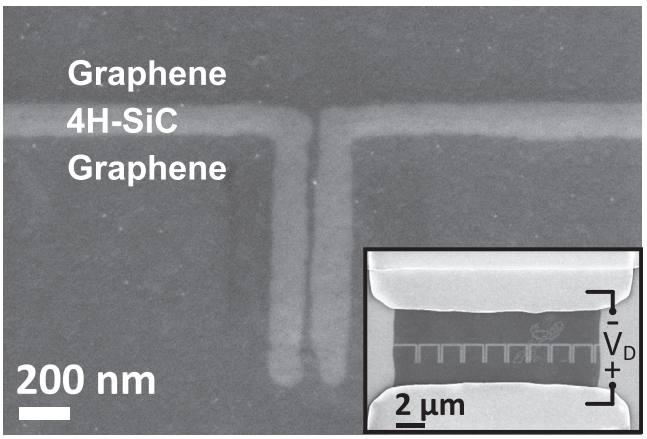

FIG. 1. Scanning electron micrograph (SEM) of a single SSD channel etched in as-grown monolayer graphene on SiC. The narrowest width of the depicted channel is 15 nm. The inset shows the SSD design used in the RF detection experiments, with nine parallel channels fabricated at the end of a 70 μm coplanar transmission line.

[a)]Author to whom correspondence should be addressed. E-mail: andreas.westlund@chalmers.se

The as-grown and H-intercalated samples were characterized using micro-Raman spectroscopy. The Raman spectra were obtained after device fabrication using a setup with a 2.33 eV (532 nm) diode pumped semiconductor laser.[21,22] Due to the BCB passivation layer, the Raman spectra were obtained by measuring through the SiC substrate resulting in reduced spatial resolution (2 μm) and spectral intensity.

The Raman spectra of the as-grown and H-intercalated samples after background subtraction of the second-order Raman scattering from the substrate are shown in Fig. 2. The as-grown and H-intercalated materials have G (2D) peaks centered on 1589 (2724) cm^{-1} and 1595 (2717) cm^{-1}, respectively. The spectrum of the as-grown sample contains a significant contribution from the CBL in the range of 1340–1640 cm^{-1}, which is absent in the H-intercalated sample, demonstrating the effect of intercalation. The observed upshift (downshift) in the G (2D) peaks upon intercalation reflects a reduction of the stress in the graphene as well as a change in carrier density. Additionally, the H-intercalated sample demonstrates a very weak D-peak at 1364 cm^{-1}. Since the D-peak in defect free graphene is forbidden in Raman scattering by momentum conservation, its presence indicates defects in the lattice. The intensity ratio I_D/I_G of the D-peak (I_D) and the G-peak (I_G) therefore defines a figure of merit regarding material quality. The intercalated layer demonstrates $I_D/I_G = 0.023$ indicating low defect density.[23–27] Such a comparison is intractable in the as-grown sample because the D-peak is obscured by the CBL spectrum.[27] The increase in linewidth from 50 cm^{-1} to 68 cm^{-1} for the 2D peak upon H-intercalation is indicative of a transition from monolayer (plus CBL) to quasi-free standing bilayer material, though there may be additional spectral broadening in both samples due to the presence of the BCB encapsulation layer.

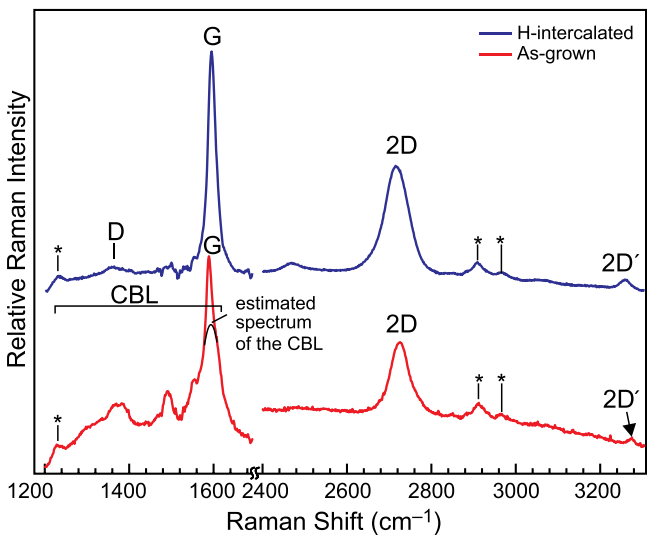

FIG. 2. Raman spectra for the as-grown and H-intercalated samples after fabrication of SSD devices. The G, 2D and D peak positions are shown. The as-grown material is monolayer graphene plus CBL, whereas the H-intercalated sample is bilayer graphene. In the as-grown material, the G-peak overlaps with the CBL spectrum; the thin solid line underneath the G peak is an estimate of the contribution of the CBL in the region of overlap. The observed intensity ratios of the G- and 2D-peaks suggest monolayer graphene in the as-grown sample and bilayer in the H-intercalated one. The peaks marked with asterisks are likely due to contribution from the BCB top film. Note the horizontal-axis break.

A nonlinear current-voltage (IV) relationship enables RF detection with SSDs. For an RF detector based on nonlinear IV characteristic, the voltage responsivity with an RF source of impedance Z_s is $\beta_{Zs} = -\frac{1}{2}R_D\gamma(1-|\Gamma|^2)$, where $R_D = dV_D/dI_D$ is the differential resistance, $\gamma = (d^2I_D/dV_D^2)/(dI_D/dV_D)$, and Γ is the reflection coefficient between source and detector.[28] At low frequencies and for $R_D \gg \mathrm{Re}(Z_s)$, the responsivity is $\beta_{Zs} \approx -2\gamma\mathrm{Re}(Z_s)$. At zero-bias, the dominating noise process is Johnson noise.[29] The noise-equivalent power is thus $\mathrm{NEP} = \sqrt{4kTR_0}/\beta_{Zs}$, where k is Boltzmann's constant, $T = 300$ K the temperature, and $R_0 = R_D(V_D = 0\,\mathrm{V})$.

DC characteristics of SSDs from the as-grown and H-intercalated sample are shown in Fig. 3. At zero bias, the as-grown sample exhibits $\gamma = 0.024\,\mathrm{V}^{-1}$ and $R_0 = 67.1\,\mathrm{k\Omega}$. At zero-bias, a low-frequency responsivity of $\beta_{50\Omega} \approx -2.4\,\mathrm{V/W}$ is expected with a $Z_s = 50\,\Omega$ source. The corresponding figures for the H-intercalated sample are $\gamma = -0.022\,\mathrm{V}^{-1}$, $R_0 = 4.21\,\mathrm{k\Omega}$, and $\beta_{50\Omega} \approx 2.2\,\mathrm{V/W}$. The non-zero γ at zero-bias in both SSDs enables zero-bias RF detection.

SSDs fabricated on as-grown and H-intercalated graphene are expected to exhibit opposite signs for $\beta_{50\Omega}$. In the as-grown sample, which is n-type, the lateral gates at forward bias ($V_D > 0\,\mathrm{V}$) act to increase carrier density and reduce R_D as shown in Fig. 3(a). In weak reverse bias ($V_D < 0\,\mathrm{V}$), carrier density is decreased and R_D increased. In the p-type H-intercalated sample, the holes are the majority carriers and the operation reversed.

The SSD on the as-grown sample exhibits a local maximum of R_D when biased at the Dirac voltage $V_{Dirac} = -70$ mV, see Fig. 3(a). A maximum R_D is expected for the V_D which brings the Fermi energy ϵ_f to the Dirac point in the material (i.e., V_{Dirac}). This corresponds to a minimum in the carrier density. The sign and value of V_{Dirac} in the as-grown sample indicate that the channel is n-type and lowly doped in qualitative agreement with the mean Fermi energy extracted from Hall measurements. For the H-intercalated sample, V_{Dirac} occurs at positive bias and is not visible within the measured range, indicating a highly p-doped graphene channel, which is also consistent with Hall data (Fig. 3(b)).

Responsivity was measured on wafer in the band 1–67 GHz using the setup shown in the inset of Fig. 4. The signal source was an Agilent 8275D. A 10 dB attenuator provided the nominal source impedance $Z_s = 50\,\Omega$. RF power was applied to the detector with a 75 μm pitch coplanar probe. The available power at the SSD input ($P_{av,SSD}$) was

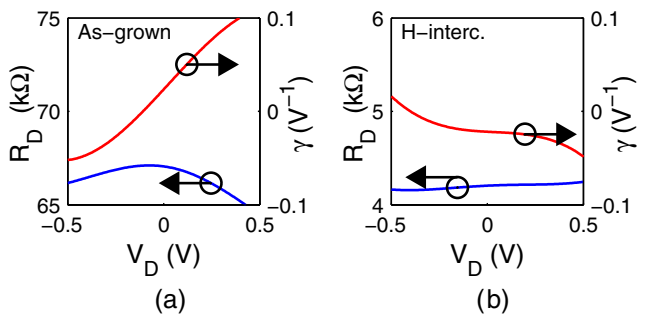

FIG. 3. Differential diode resistance (R_D) and $\gamma = (d^2I_D/dV_D^2)/(dI_D/dV_D)$ for nine-channel SSDs on the (a) as-grown sample and the (b) H-intercalated sample.

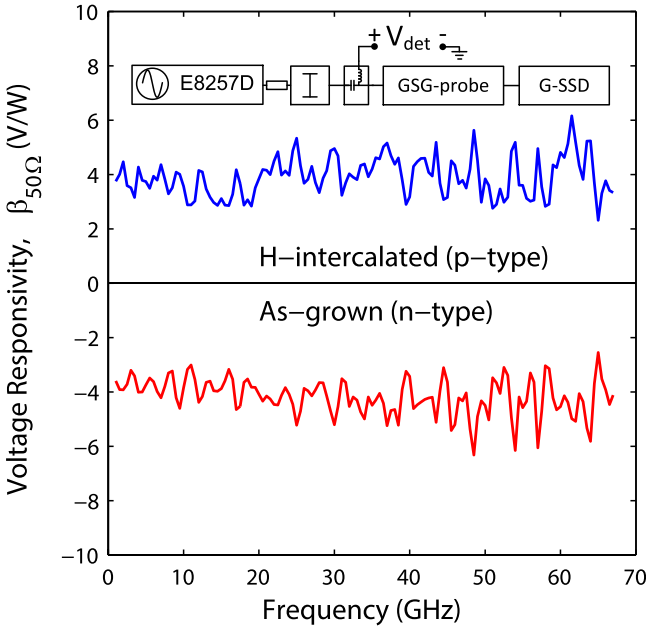

FIG. 4. Voltage responsivity versus frequency for SSDs on the as-grown and H-intercalated sample. The inset shows the on-wafer measurement setup.

calculated by subtracting measured probe loss from the power measured at the probe input with an Agilent E4419B power meter using sensors HP8487A (1–50 GHz) and V8486A (50–67 GHz). $P_{av,SSD}$ ranged from 24 μW to 3 μW in the measured band. The DC voltage V_{det} was measured with a Keithley 2000 multimeter, and the responsivity was then calculated as $\beta_{50\Omega} = V_{det}/P_{av,SSD}$.

The measured high-frequency responsivity is presented in Fig. 4. The SSDs exhibit an average $\beta_{50\Omega}$ of 3.9 and −4.2 V/W from 1 to 67 GHz for the H-intercalated and as-grown samples, respectively. In correspondence with the DC-measurements, $\beta_{50\Omega}$ for the two samples are of similar magnitude but with different signs. The opposite sign between the as-grown (n-type) and H-intercalated (p-type) samples show that the SSD detectors operate in the intended way as indicated in Fig. 3.

The estimated NEP up to 67 GHz is plotted in Fig. 5. The average NEP is 2.2 and 8.2 nW/Hz$^{1/2}$ for the H-intercalated and as-grown samples, respectively. While both SSDs demonstrate similar $\beta_{50\Omega}$, the estimated NEP is considerably lower in the H-intercalated sample due to the lower R_{sh} and R_0 compared to the as-grown sample.

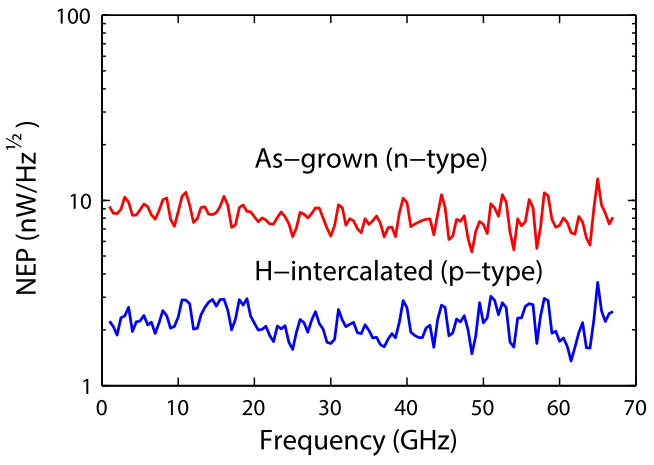

FIG. 5. Estimated NEP for the SSDs fabricated from the two graphene samples.

The graphene SSD presented in this study can be improved for zero-bias microwave detection. First, the SSD channel fabrication can be developed for better edge acuity (Fig. 1). The varying channel width causes a non-uniform electric field across the channel leading to reduced responsivity.[14] On the H-intercalated sample, a single-channel SSD exhibited $\gamma = -0.1\,V^{-1}$, $R_0 = 9.2\,\text{k}\Omega$, and thus an expected $\beta_{50\Omega} = 10\,\text{V/W}$. With the same γ, nine parallel channels and an SSD driven by a source with the free-space impedance $Z_s = 377\,\Omega$, a low-frequency responsivity $\beta_{377\Omega} = -2\gamma Z_s = 75\,\text{V/W}$ and NEP $= 54\,\text{pW/Hz}$ can be expected. Second, the width of the isolating trenches can be reduced to enhance gate-to-channel coupling thus increasing γ.[14] The non-optimized graphene SSDs exhibit similar performance compared to more optimized InAs SSDs with $\gamma = 0.35\,\text{V}^{-1}$ and $R_0 = 15\,\text{k}\Omega$ per channel.[12] Even though the graphene SSDs in this study were only characterized up to 67 GHz, the results point to the graphene SSD as a potential candidate for millimeter wave or even terahertz detection. Graphene SSDs are potentially of interest for transparent electronics.[30,31] Furthermore, the use of epitaxial growth of graphene on commercially available 4H-SiC wafers makes the SSD detectors viable for volume production of detector arrays.

In conclusion, self-switching diodes (SSDs) using epitaxial graphene on 4H-SiC have been demonstrated. Zero-bias graphene SSD detectors showed promising results using on-wafer measurements up to 67 GHz. Graphene SSDs on H-intercalated graphene exhibited a flat voltage responsivity of 3.9 V/W and an NEP of 2.2 nW/Hz$^{1/2}$.

This work was supported by the Swedish Research Council (VR 621-2012-4633) and European Science Foundation (ESF) under the EUROCORES Program EuroGRAPHENE (EPIGRAT). We also acknowledge support from the Swedish Foundation for Strategic Research (SSF), project "Graphene based high-frequency electronics" (RE10-0077), and the Knut and Alice Wallenberg Foundation (KAW), project "Swedish Graphene Initiative."

[1]K. I. Bolotin, K. J. Sikes, Z. Jiang, M. Klima, G. Fudenberg, J. Hone, P. Kim, and H. L. Stormer, Solid State Commun. **146**, 351 (2008).
[2]R. Appleby and H. B. Wallace, IEEE Trans. Antennas Propag. **55**, 2944 (2007).
[3]Z. Zhang, R. Rajavel, P. Deelman, and P. Fay, IEEE Microw. Wireless Compon. Lett. **21**, 267 (2011).
[4]D. Schoenherr, C. Bleasdale, T. Goebel, C. Sydlo, H. L. Hartnagel, R. Lewis, and P. Meissner, in *35th International Conference on Infrared, Millimeter, Terahertz Waves* (IEEE, 2010).
[5]A. Zak, M. A. Andersson, M. Bauer, A. Lisauskas, H. G. Roskos, and J. Stake, in *2014 39th International Conference on Infrared, Millimeter, Terahertz Waves* (IEEE, 2014).
[6]A. M. Song, M. Missous, P. Omling, A. R. Peaker, L. Samuelson, and W. Seifert, Appl. Phys. Lett. **83**, 1881 (2003).
[7]F. Al-Dirini, F. M. Hossain, A. Nirmalathas, and E. Skafidas, Sci. Rep. **4**, 3983 (2014).
[8]F. Al-Dirini, F. M. Hossain, A. Nirmalathas, and E. Skafidas, Nanoscale **6**, 7628 (2014).
[9]J. Kettle, R. M. Perks, and R. T. Hoyle, Electron. Lett. **45**, 79 (2009).
[10]C. Balocco, A. M. Song, M. Åberg, A. Forchel, T. González, J. Mateos, I. Maximov, M. Missous, A. A. Rezazadeh, J. Saijets, L. Samuelson, D.

Wallin, K. Williams, L. Worschech, and H. Q. Xu, Nano Lett. **5**, 1423 (2005).
[11]P. Sangaré, G. Ducournau, B. Grimbert, V. Brandli, M. Faucher, C. Gaquière, A. Íñiguez-de-la-Torre, I. Íñiguez-de-la-Torre, J. F. Millithaler, J. Mateos, and T. González, J. Appl. Phys. **113**, 034305 (2013).
[12]A. Westlund, P. Sangaré, G. Ducournau, P.-A. Nilsson, C. Gaquière, L. Desplanque, X. Wallart, and J. Grahn, Appl. Phys. Lett. **103**, 133504 (2013).
[13]C. Balocco, S. R. Kasjoo, X. F. Lu, L. Q. Zhang, Y. Alimi, S. Winnerl, and A. M. Song, Appl. Phys. Lett. **98**, 223501 (2011).
[14]A. Westlund, I. Iñiguez-de-la-Torre, P.-Å. Nilsson, T. González, J. Mateos, P. Sangaré, G. Ducournau, C. Gaquière, L. Desplanque, X. Wallart, and J. Grahn, Appl. Phys. Lett. **105**, 093505 (2014).
[15]A. Westlund, P. Sangaré, G. Ducournau, I. Iñiguez-de-la-Torre, P.-Å. Nilsson, C. Gaquière, L. Desplanque, X. Wallart, J. F. Millithaler, T. González, J. Mateos, and J. Grahn, Solid State Electron. **104**, 79 (2015).
[16]L. Biedermann, M. Bolen, M. Capano, D. Zemlyanov, and R. Reifenberger, Phys. Rev. B **79**, 125411 (2009).
[17]C. Riedl, C. Coletti, T. Iwasaki, A. A. Zakharov, and U. Starke, Phys. Rev. Lett. **103**, 246804 (2009).
[18]J. A. Robinson, M. Hollander, M. Labella, K. A. Trumbull, R. Cavalero, and D. W. Snyder, Nano Lett. **11**, 3875 (2011).
[19]J. Hassan, C. Virojanadara, A. Meyer, I. G. Ivanov, J. I. Flege, S. Watcharinyanon, J. Falta, L. I. Johansson, and E. Janzén, Mater. Sci. Forum **717–720**, 605 (2012).
[20]M. Winters, J. Hassan, H. Zirath, E. Janzeń, and N. Rorsman, J. Appl. Phys. **113**, 193708 (2013).
[21]M. Winters, O. Habibpour, I. G. Ivanov, J. Hassan, E. Janzén, H. Zirath, and N. Rorsman, Carbon **81**, 96 (2015).
[22]I. G. Ivanov, J. U. Hassan, T. Iakimov, A. A. Zakharov, R. Yakimova, and E. Janzén, Carbon **77**, 492 (2014).
[23]A. C. Ferrari, J. C. Meyer, V. Scardaci, C. Casiraghi, M. Lazzeri, F. Mauri, S. Piscanec, D. Jiang, K. S. Novoselov, S. Roth, and A. K. Geim, Phys. Rev. Lett. **97**, 187401 (2006).
[24]A. Eckmann, A. Felten, A. Mishchenko, L. Britnell, R. Krupke, K. S. Novoselov, and C. Casiraghi, Nano Lett. **12**, 3925 (2012).
[25]A. Ferrari and J. Robertson, Phys. Rev. B **61**, 14095 (2000).
[26]A. C. Ferrari, Solid State Commun. **143**, 47 (2007).
[27]F. Fromm, M. H. Oliveira, Jr., A. Molina-Sánchez, M. Hundhausen, J. M. J. Lopes, H. Riechert, L. Wirtz, and T. Seyller, New J. Phys. **15**, 043031 (2013).
[28]A. M. Cowley and H. O. Sorensen, IEEE Trans. Microw. Theory Tech. **14**, 588 (1966).
[29]C. Balocco, S. R. Kasjoo, L. Q. Zhang, Y. Alimi, and A. M. Song, Appl. Phys. Lett. **99**, 113511 (2011).
[30]S.-K. Lee, H. Y. Jang, S. Jang, E. Choi, B. H. Hong, J. Lee, S. Park, and J.-H. Ahn, Nano Lett. **12**, 3472 (2012).
[31]S. Lee, K. Lee, C.-H. Liu, G. S. Kulkarni, and Z. Zhong, Nat. Commun. **3**, 1018 (2012).